Subband Index Carrierless Amplitude and Phase Modulation for Optical Communications

Subband Index Carrierless Amplitude and Phase Modulation for Optical Communications

Kabiru O. Akande, *Student Member, IEEE* and Wasiu O. Popoola, *Senior Member, IEEE*

***Abstract*—Subband index carrierless amplitude and phase modulation (SI-CAP) is proposed and investigated in this work to improve the performance of multi-band CAP (m-CAP). The bit-error-rate (BER) analysis of the proposed SI-CAP is derived and verified through computer simulations. A detection scheme is also developed for SI-CAP which achieves maximum likelihood (ML) performance at a significantly lower complexity. In addition, an experimental demonstration of the proposed SI-CAP is carried out for optical communication systems. Furthermore, adaptive equalization technique is implemented to further enhance the performance gain of SI-CAP. It is shown that for the same order of complexity, the SI-CAP exhibits higher spectral and energy efficiency in comparison to m-CAP. Therefore, the performance gain of SI-CAP along with its design flexibility make it a suitable candidate for optical communication systems.**

***Index Terms*—Multi-band carrierless amplitude and phase modulation (m-CAP), optical communication, visible light communication (VLC), index modulation (IM), step-index plastic optical fibre (SI-POF), adaptive equalization.**

I. Introduction

There is an ever increasing demand for high speed data connection due to unprecedented growth in broadband communication and the expected ubiquitous connectivity of smart devices. This demand requires communication technologies that can support the existing overcrowded radio frequency (RF) communication to meet the future data traffic. Optical communication is one of such techniques as it offers huge spectrum with low cost devices [1]. Step-index plastic optical fibre (SI-POF) has received high interest in optical communication due to its low cost, ease of installation and resilience to electromagnetic interference [2]. In addition, visible light communication (VLC) has become an emerging technology in the field of optical wireless communication (OWC) [3]. The VLC can leverage existing lighting fixtures for data communication and its benefits include the use of low-cost devices, availability of huge spectrum and high security, among others [3], [4].

The commercially available white light emitting diodes (LEDs) that are predominantly employed for illumination and VLC have small modulation bandwidth and creates a bottleneck in achieving high data rate. Furthermore, high data rate transmission over SI-POF results in inter-symbol interference (ISI) due to its limited bandwidth-length product, typically 45 MHz $\times$ 100 m. [5], [6]. Carrierless amplitude and phase modulation (CAP) is suitable for improving the spectral efficiency of the foregoing optical communication systems. Recent experimental works have demonstrated Gb/s data rate for short range POF/VLC communication with CAP [2], [7]–[9].

The CAP performance is sensitive to the non-linearity effect of the VLC devices and that of optical fibre. Complex cascaded equalizers have been deployed to address the resulting intersymbol interference (ISI) but this approach eliminates the inherent low-complexity advantage of CAP [8]. A solution that avoids equalization complexity has recently been proposed where multiple low rate CAP symbols are transmitted through groups of LEDs using spatial modulation technique to realise high spectral efficiency [10]. The spatial modulation solution has been experimentally demonstrated to offer improved data rate and spectral efficiency without the need for equalizers [11]. The problem with the spatial approach is that it requires distinct channel gains for optimal performance and this might not be available especially for mobile VLC systems [12].

Alternatively, the available link bandwidth can be subdivided to realise multi-band CAP (m-CAP) with improved tolerance towards channel non-linearity effect [13], [14]. The m-CAP scheme has been experimentally demonstrated to offer improved BER performance for optical communication systems [14], [15]. Despite its BER improvement, the m-CAP scheme does not improve the transmission efficiency, defined as the number of bits encoded per transmitted symbol, of the conventional CAP system. In addition, m-CAP suffers the same high PAPR problem inherent in multi-carrier systems. Therefore, subband index CAP (SI-CAP) is introduced in this paper to improve on the spectral and energy efficiency of the m-CAP system.

The SI-CAP works by modulating some of the subbands (termed active subbands) of m-CAP with data symbols. It then make up on the lost spectral efficiency by encoding additional bits in the selection of the active/inactive subband indices. Additionally, a detection scheme is developed for SI-CAP that achieves maximum likelihood (ML) performance at lower complexity. Furthermore, as will be shown, a proper configuration of the SI-CAP system parameters results in higher throughput beyond the maximum $\log_2(M)$ bits per channel use (bpcu) possible in m-CAP. The performance gain of SI-CAP is demonstrated using theoretical analysis, simulations and experimental demonstrations in both VLC and SI-POF. An adaptive equalization technique is further implemented which results in higher gain for the proposed SI-CAP.

During each symbol duration, the SI-CAP scheme transmits unique M-QAM symbol on each N_a active subbands out of the total N subbands available. Though, there are ${}^{N}C_{N_\mathrm{a}}$

The authors are with the LiFi Research and Development Centre, Institute for Digital Communications, School of Engineering, The University of Edinburgh, Edinburgh EH9 3JL, U.K. (e-mail: k.akande@ed.ac.uk; w.popoola@ed.ac.uk).

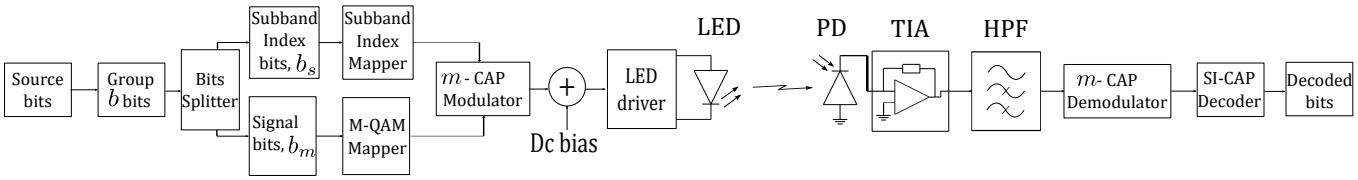

Fig. 1. The schematic block diagram of the proposed SI-CAP transceiver for VLC link.

possible combinations/ways for selecting N_{a} out of N, only $N_{\mathrm{u}} = 2^{\lfloor \log_2 \binom{N}{N_{\mathrm{a}}} \rfloor}$ combinations can be employed for carrying information bits where $\lfloor \cdot \rfloor$ is the floor function. Thus, the total number of bits that can be encoded in the subband domain of the proposed SI-CAP is $\log_2(N_{\mathrm{u}})$.

The main contributions of this paper are therefore summarized as follows: 1.) A novel SI-CAP scheme which improves on the energy and spectral efficiency of the conventional m-CAP is proposed and investigated; 2.) a detection scheme that achieves ML performance at lower complexity is presented along with the BER analysis of SI-CAP; 3.) experimental demonstration of SI-CAP is then performed to validate the performance gains of the technique in optical communication systems.

The rest of the paper is organized as follows: the description of the proposed SI-CAP model is detailed in section II while its detection schemes along with the theoretical analysis are developed and presented in Section III. The simulation and experimental results are respectively discussed in Section IV and V while Section VI concludes the paper.

II. Description of SI-CAP

The system model for the proposed SI-CAP is detailed in this Section starting with a brief illustration of m-CAP scheme.

A. System Description of m-CAP

Multiple subband CAP, m-CAP, is generated by modulating unique $\log_2(M)$ bits on each of the N subbands of an m-CAP signal [11], [15]. For each subband, the data bits are first mapped to corresponding M-QAM symbol and subsequently upsampled. The upsampled symbols are then separated into the real and imaginary parts before being passed to the in-phase ($h(t)$) and quadrature ($\bar{h}(t)$) filters, respectively. The impulse responses of $h(t)$ and $\bar{h}(t)$ are orthogonal, form a Hilbert pair and are respectively generated as the product of cosine and sine waves with a root-raised cosine filter (RRCF) [8]. The transmit filters for the nth subband can be expressed as:

$$h_n(t) = g(t)\cos(2\pi f_{\mathrm{c},n} t) \tag{1}$$

and

$$\bar{h}_n(t) = g(t)\sin(2\pi f_{\mathrm{c},n} t) \tag{2}$$

where $g(t)$ is the RRCF and $f_{\mathrm{c},n}$ is the center frequency of the nth subband given as:

$$f_{\mathrm{c},n} = (2n-1)f_{\mathrm{c}}. \tag{3}$$

The $\{f_{\mathrm{c},n}\}$ are chosen such that the subbands of m-CAP do not overlap. At the output of the transmit filters, the m-CAP signals are added together with a DC-bias to ensure non-negativity and subsequently modulated on the intensity of the transmitting optical source. Optical radiation from the transmitter is directly detected by the receiving PD, passed through a transimpedance amplifier for current-to-voltage conversion and a high pass filter to remove the DC component. The resulting signal is then passed through the conjugate, time-reversed version of the transmit filters for match filtering and subsequently decoded using M-QAM demapper.

B. SI-CAP System Description

The proposed SI-CAP system configuration is represented as $\Omega = \left\langle \binom{N}{N_{\mathrm{a}}} \right\rangle_M^{\mathcal{T}}$ where N, N_{a}, M and $\mathcal{T}$ respectively represent the total number of subbands, number of active subbands, QAM constellation order, and the transmission efficiency of the system in bpcu. The previously described m-CAP can be regarded as a special case of SI-CAP where $N_{\mathrm{a}} = N$. In order to generate the SI-CAP signal, the total b bits to be transmitted is split into two groups consisting of the symbol bits, $b_{\mathrm{m}} = N_{\mathrm{a}}\log_2(M)$ and the subband bits, $b_{\mathrm{s}} = \log_2(N_{\mathrm{u}})$ as shown in Fig. 1. The b_{s} bits are then used to select the appropriate subband indices, $S_{n_{\mathrm{u}}}$, out of the total possible set, $\mathcal{S}$. The set $\mathcal{S} = \left\{S_{n_{\mathrm{u}}}\right\}_{n_{\mathrm{u}}=1}^{N_{\mathrm{u}}}$ can also be referred to as the subband constellation while $S_{n_{\mathrm{u}}} = \left\{S_{n_{\mathrm{u}}}^{n_{\mathrm{a}}}\right\}_{n_{\mathrm{a}}=1}^{N_{\mathrm{a}}}$ can be referred to as the subband symbol. The b_{m} bits are then mapped to the subbands corresponding to $S_{n_{\mathrm{u}}}$ while zeros are placed on the remaining subbands i.e the remaining subbands are not modulated with data symbols.

The process of generating SI-CAP signal is illustrated with an example as follows: consider a total of 4 subbands in which 2 are active. There are 6 (that is, ${}^4C_2$) different ways or combinations of selecting the 2 active subbands, out of which only $N_{\mathrm{u}} = 4$ (that is, $2^{\lfloor \log_2({}^4C_2) \rfloor}$) can be chosen. Thus, $b_{\mathrm{s}} = 2$ bits can be encoded in the selection of the $N_{\mathrm{u}} = 4$ subband combinations. The active subbands corresponding to the chosen combination are then encoded with data symbols from QAM constellation. For this example, the system configuration is $\Omega = \left\langle \binom{4}{2} \right\rangle_4^{1.5}$. To transmit bits $b = \text{`}011001\text{'}$, the first $b_{\mathrm{s}}$ bits, `01', is used for selecting the $S_{n_{\mathrm{u}}}$ which corresponds to $S_2 = \{1, 3\}$ using Table I. This means that only the 1st and 3rd subbands will carry information while no information will be carried on the 2nd and 4th subbands. Notice that the entries of $\mathcal{S}$ have been arbitrarily selected from the total number of possible combinations. The remaining b_{m} bits, `1001', is then used to select the appropriate QAM symbols from the QAM constellation, $\mathcal{M}$, which in this case

TABLE I
SI-CAP MAPPING PROCESS FOR $\Omega = \langle {}^{4}_{2} \rangle^{1.5}_{4}$

Possible subband constellation	b_s bits	Selected subband constellation, $\mathcal{S}$	Signal bits	Signal constellation, $\mathcal{M}$
1, 2	00	1, 2	00	$+1+j$
1, 3	01	1, 3	01	$-1+j$
1, 4	10	1, 4	10	$-1-j$
2, 3	11	2, 3	11	$+1-j$
2, 4				
3, 4				

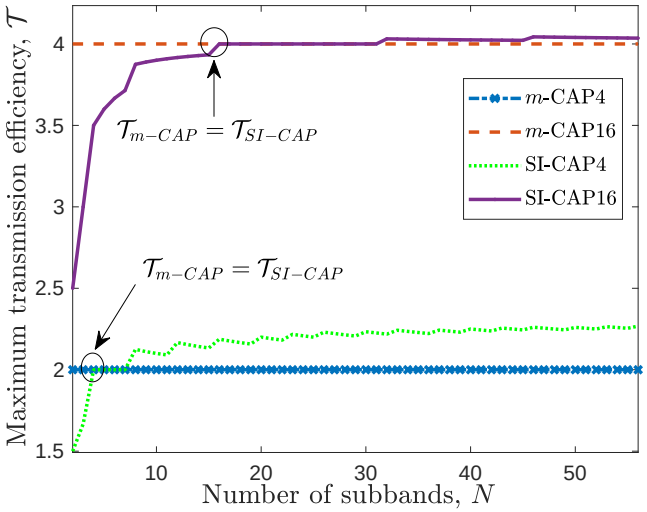

Fig. 2. The maximum transmission efficiency, $\mathcal{T}$, in bpcu achievable by SI-CAP and m-CAP as number of subbands, N, increases.

correspond to symbol $-1-j$ and $-1+j$. Thus, the signal sent to the m-CAP modulator is

$$\mathbf{x} = \begin{bmatrix} -1-j & 0 & -1+j & 0 \end{bmatrix}^T. \tag{4}$$

The transmission efficiency of SI-CAP, which is the number of bits encoded per SI-CAP symbol in bits per channel use (bpcu), can thus be expressed as:

$$\mathcal{T}_{SI-CAP} = \frac{b_s + b_m}{N} \tag{5}$$

$$= \frac{\left\lfloor \log_2 \left({}^{4}C_2 \right) \right\rfloor + N_a \log_2(M)}{N}. \tag{6}$$

Both the transmission efficiency of SI-CAP and m-CAP are compared and shown in Fig. 2 for $M = 4$ and 16. The figure shows that $\mathcal{T}_{\text{SI-CAP}}$ exceeds the maximum limit of $\log_2(M)$ possible for $\mathcal{T}_{m\text{-CAP}}$. It can also be deducted from the Fig. 2 that the condition $N \geq M$ has to be satisfied for $\mathcal{T}_{\text{SI-CAP}}$ to be equal to $\mathcal{T}_{m\text{-CAP}}$. This is shown by circles in Fig. 2 for $M = 4$ and 16. Due to the condition $N \geq M$, the number of subbands required for SI-CAP to improve on $\mathcal{T}_{m\text{-CAP}}$ increases with increasing M. This requirement increases the complexity of the resulting system for high value of M.

III. Detection Schemes for SI-CAP

Due to the extra bits carried by the index of the SI-CAP subbands, the conventional m-CAP detector can not be successfully applied. Therefore, three detectors are investigated for the proposed SI-CAP scheme. The received SI-CAP signal at the output of the m-CAP demodulator, considering line-of-sight (LOS) channel gain h, can be expressed as:

$$\mathbf{r} = \xi \Re P_t h \mathbf{x}^m_{n_u} + \mathbf{w} \tag{7}$$

where r_n, $x^m_{n_u,n}$ and w_n are the components of the $N \times 1$ vectors $\mathbf{r}$, $\mathbf{x}^m_{n_u}$ and $\mathbf{w}$, respectively. The $x^m_{n_u,n}$ is the symbol transmitted on the nth subband and is either zero or belongs to one of the M-QAM symbols as shown in (4). The total transmit optical power is denoted as P_t, $\xi = N/N_a$ is the scaling factor required to keep the total transmit optical power constant irrespective of the system configuration while $\Re$ is the responsivity of the photodetector. The noise component, w_n, for the nth subband is modelled as additive white Gaussian noise (AWGN) with zero mean and double-sided power spectral density $N_0/2$. The received signal in (7) can be re-written as

$$\mathbf{r} = \zeta^m_{n_u} + \mathbf{w} \tag{8}$$

where $\zeta^m_{n_u} = \xi \Re P_t h \mathbf{x}^m_{n_u}$.

A. SI-CAP with Maximum Likelihood Detector (MLD)

The performance analysis of the proposed SI-CAP is derived based on the ML detector. The MLD is the optimum detector for SI-CAP considering the fact that its symbols, $\{\mathbf{x}^m_{n_u}\}$, are equiprobable with $p(\mathbf{x}^m_{n_u}) = 1/N_u M^{N_a}$. As a result, the decision criteria for MLD can be expressed as [16]:

$$\hat{\mathbf{x}}^m_{n_u} = \arg \max_{n_u, m} p(\mathbf{r}, \zeta^m_{n_u}) \tag{9}$$

where

$$p(\mathbf{r}, \zeta^m_{n_u}) = \frac{1}{(2\pi N_0)^{N/2}} \exp\left[-\frac{\left\| \mathbf{r} - \zeta^m_{n_u} \right\|^2}{2N_0} \right] \tag{10}$$

due to the AWGN channel. The criterion in (9) can be reduced to

$$\hat{\mathbf{x}}^m_{n_u} = \arg \min_{n_u, m} D(\mathbf{r}, \zeta^m_{n_u}) \tag{11}$$

where

$$D(\mathbf{r}, \zeta^m_{n_u}) = \left\| \mathbf{r} - \zeta^m_{n_u} \right\|^2. \tag{12}$$

The pairwise error probability (PEP), which is the probability of error for detecting $\tilde{\mathbf{x}}$ when $\mathbf{x}$ has been transmitted, is employed in the derivation of the SI-CAP error probability. Both the subband index and symbol bits are jointly detected by the MLD. The minimum Euclidean distance criterion of (11) becomes

$$D(\mathbf{r}, \zeta^m_{n_u}) = \|\mathbf{w}\|^2 \tag{13}$$

in case the detector makes the correct decision, otherwise

$$D(\mathbf{r}, \tilde{\zeta}^m_{n_u}) = \left\| \zeta^m_{n_u} - \hat{\zeta}^m_{n_u} - \mathbf{w} \right\|^2. \tag{14}$$

Using (13) and (14), the PEP can be derived as:

$$\begin{aligned} PEP_{\text{SI-CAP}} &= p(\mathbf{x}^m_{n_u} \rightarrow \tilde{\mathbf{x}}^m_{n_u}) \\ &= p(D(\mathbf{r}, \zeta^m_{n_u}) > D(\mathbf{r}, \tilde{\zeta}^m_{n_u})) \\ &= Q\left(\sqrt{\frac{(\xi P_t \Re)^2}{2N_0} \left\| h \left(\mathbf{x}^m_{n_u} - \tilde{\mathbf{x}}^m_{n_u} \right) \right\|^2} \right). \end{aligned} \tag{15}$$

The PEP of (15) is used to obtain an upper bound on the BER of SI-CAP, as shown in (16), by considering all possible

$$BER_{\text{SI-CAP}} \leq \frac{1}{N_{\text{u}} M^{N_{\text{a}}} \log_2(N_{\text{u}} M^{N_{\text{a}}})} \sum_{n_{\text{u}}=1}^{N_{\text{u}}} \sum_{m=1}^{M^{N_{\text{a}}}} \sum_{\tilde{n}_{\text{u}}=1}^{N_{\text{u}}} \sum_{\tilde{m}=1}^{M^{N_{\text{a}}}} N_H(b_{mn_{\text{u}}}, \tilde{b}_{mn_u}) Q\left(\sqrt{\frac{(\xi P_t \Re)^2}{2N_0} \left\| h\left(\mathbf{x}_{n_{\text{u}}}^m - \tilde{\mathbf{x}}_{n_{\text{u}}}^m\right)\right\|^2}\right). \tag{16}$$

$N_{\text{u}} M^{N_{\text{a}}}$ symbol combinations using union bound technique [17, p. 261–262]. The $\mathcal{N}_H(b_{mn_{\text{u}}}, \tilde{b}_{mn_u})$ in (16) represents the number of erroneous bits when symbol $\tilde{\mathbf{x}}$ is detected instead of the transmitted symbol $\mathbf{x}$.

Though the optimum detector for SI-CAP is MLD, its computational complexity is prohibitive as it searches $N_{\text{u}} M^{N_{\text{a}}}$ symbol combinations in order to make decision. As a result, two lower complexity detectors are further investigated.

B. SI-CAP with Log-Likelihood Ratio Detector (LLR))

The LLR computes the logarithm of the ratio between the a *posteriori* probabilities of the SI-CAP symbols in each subband considering the fact that they are either zero or drawn from $\mathcal{M}$. Thus, the LLR is formulated as [16]:

$$\chi_n = \ln \frac{\sum_{i=1}^{M} \Pr(x_n = \mathfrak{m}_i | r_n)}{\Pr(x_n = 0 | r_n)} \tag{17}$$

where $\mathfrak{m}_i \in \mathcal{M}$. Using Bayes' theorem, (17) can be written as:

$$\chi_n = \ln \frac{\sum_{i=1}^{M} \Pr(r_n | x_n = \mathfrak{m}_i) \Pr(x_n = \mathfrak{m}_i)}{\Pr(r_n | x_n = 0) \Pr(x_n = 0)}. \tag{18}$$

Given the AWGN corrupted channel,

$$\Pr(r_n | x_n = \mathfrak{m}_i) = \frac{1}{(2\pi N_0)^{1/2}} \exp\left[-\frac{|r_n - \mathfrak{m}_i h|^2}{2N_0}\right] \tag{19}$$

while

$$\Pr(r_n | x_n = 0) = \frac{1}{(2\pi N_0)^{1/2}} \exp\left[-\frac{|r_n|^2}{2N_0}\right]. \tag{20}$$

Therefore, considering the fact that $\Pr(r_n | x_n = \mathfrak{m}_i) = N_{\text{a}}/N$ and $\Pr(r_n | x_n = 0) = (N - N_{\text{a}})/N$, the expression in (18) can be expressed as:

$$\chi_n = \ln\left(\frac{N_{\text{a}}}{N - N_{\text{a}}}\right) + \frac{|r_n|^2}{N_0} + \ln\left(\sum_{i=1}^{M} \exp\left[-\frac{|r_n - \mathfrak{m}_i h|^2}{2N_0}\right]\right). \tag{21}$$

To avoid computational overflow when computing the last term of (21), the Jacobian logarithm is employed [18], [19]. The indices of the first N_{a} entries of the computed $\{\chi_n\}$ when sorted in descending order correspond to the indices of the active subbands, $S_{n_{\text{u}}}$. Thereafter, M-QAM decoder is used to decode the symbols on the detected active subbands.

It can be seen from (21) that the complexity of LLR is of $O(NM)$, the same as the conventional m-CAP. In addition, though the LLR is a near-ML decoder as it does not use all the possible combinations of symbols, it will be shown in the results section that it does achieve the same error rate performance as the MLD.

Finally, it is possible for LLR to detect some $S_{n_{\text{u}}} \notin \mathcal{S}$ when the noise variance is very high. In such cases, the detected indices can be randomly mapped to any entry of $\mathcal{S}$ since it is already an error event.

C. SI-CAP with Low Complexity Detector (LCD)

In comparison to MLD, the LLR achieves the same solution at significantly lower complexity. However, LLR requires the knowledge of the noise variance and is susceptible to computational overflow [16], [19]. In order to address these concerns, a novel low complexity detection (LCD) scheme is proposed. The LCD makes use of prior knowledge of the constellation by directly comparing the received symbol in each subband to the entries of $\mathcal{M}$. The formulation for LCD can be expressed as:

$$\boldsymbol{\lambda}_{n,i} = \min_i |r_n - \mathfrak{m}_i h|^2. \tag{22}$$

The expression in (22) stores both the minimum value, λ_n and its corresponding index, $\lambda_{n,i}$. Consequently, the subbands corresponding to the first N_{a} entries of $\{\lambda_n\}$ when sorted in ascending order are chosen as the active subbands. In addition, the $\{\mathfrak{m}_i\}$ with $\{\lambda_{n,i}\}$ that correspond to those N_{a} entries are chosen as the symbols on the active subbands. Thus, it can be seen that the complexity of LCD is also of $O(NM)$ but with less number of computations in comparison with LLR. This is because the LCD of (22) only computes a part of the last term of (21) to complete its detection process. Whereas, the LLR detection still require M-QAM decoding after evaluating all the terms in (21). Furthermore, the LCD is not susceptible to computational overflow like LLR and does not contain the noise variance in its expression. In addition, LCD achieves the same performance as the ML and LLR detectors.

However, the LCD is also liable to decide on some $S_{n_{\text{u}}} \notin \mathcal{S}$. In such cases, the random mapping solution employed for LLR is implemented.

IV. Simulation Results and Discussions

In the results presented in this section, the electrical signal-to-noise ratio per bit is defined as $\gamma_b = \frac{(\xi P_t \Re)^2}{\mathcal{T} N_0}$ where $\mathcal{T}$ is $\log_2(M)$ for m-CAP and it is as defined in (6) for SI-CAP [20].

The theoretical expression obtained for SI-CAP is validated in Fig. 3 using different M-QAM constellations and system configurations. The analysis shows excellent match with the simulation for both $\mathcal{T}$ = 1, 2 and 3.5 bpcu. The slight difference between the analysis and simulation observed at low SNR is due to the union bound technique employed for the analytical derivation. At BER of 10^{-4}, the proposed SI-CAP requires γ_b of 6.5, 8 and 12 dB to achieve transmission efficiencies of 1, 2 and 3.5 bpcu, respectively. It is also shown that the LLR achieves the same performance as the MLD at a reduced complexity. Similarly, the LCD also achieve the same performance as the MLD but at reduced number of computations in comparison to LLR. Furthermore, the LCD is not susceptible to computational overflow and does not require the knowledge of the noise variance. Hence, it can be concluded that the LCD is the best detection scheme

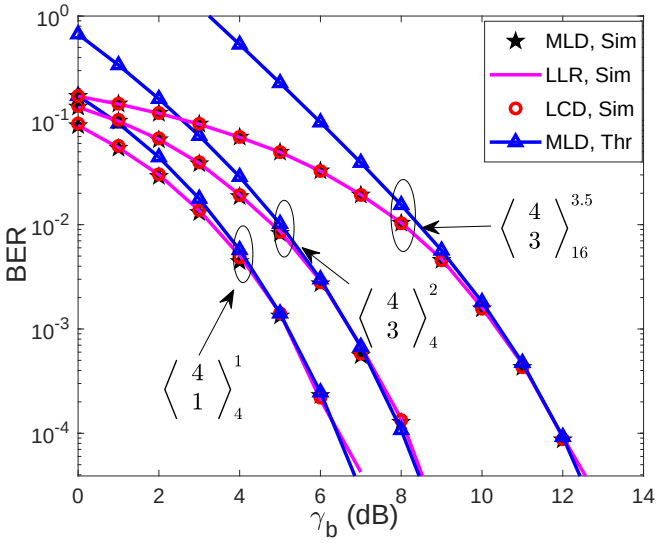

Fig. 3. Comparison of the performance of SI-CAP detectors and validation of the derived analysis using different system configurations. Sim: Simulation; Thr: Theoretical analysis

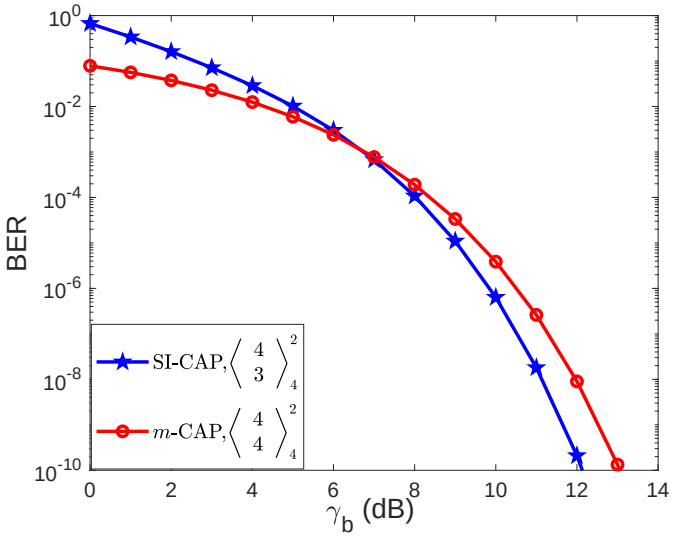

Fig. 4. The BER performance comparison of SI-CAP and m-CAP in AWGN channel, $\mathcal{T}$ = 2 bpcu.

in terms of performance and complexity considerations for the proposed SI-CAP. Also, it can be inferred that the same analysis for MLD is valid for both LLR and LCD since both detectors achieve the same performance as MLD.

The BER performance of the proposed SI-CAP and the conventional m-CAP in AWGN channel is shown in Fig. 4 for $\mathcal{T}$ = 2 bpcu. The SI-CAP has a performance gain of about 1 dB over m-CAP at high SNR. This shows the power efficiency of SI-CAP over the conventional m-CAP. The figure also shows that SI-CAP has a slight performance loss at low SNR which might be attributed to its joint detection of both the subband index and symbol bits as compared to only the symbol bits in m-CAP. The joint detection might result in error propagation as an erroneous detection of the active subband will most likely result in symbol bits error. However, SI-CAP achieves better performance at high SNR when the likelihood of error propagation reduces.

The effect of bandwidth-limited LED employed in VLC on SI-CAP and m-CAP is investigated using a first-order low pass filter (LPF) model for the LED response [15]. The result is shown in Fig. 5 by comparing the γ_b required to achieve BER of 10^{-5} for a range of spectral efficiencies, η. The proposed SI-CAP has better performance than the conventional m-CAP as it requires lower γ_b to achieve the same spectral efficiency. For example, to achieve BER of 10^{-5} at η = 5 bits/s/Hz, SI-CAP requires about 13.2 dB compare to 15.7 dB required by m-CAP as shown in Fig. 5 (a). This results in an γ_b gain of 2.5 dB for SI-CAP over m-CAP. Alternatively, with an γ_b of 15 dB, SI-CAP achieves η of 7.4 bits/s/Hz in comparison to 4.75 bits/s/Hz achieved by m-CAP which leads to η gain of 2.65 bits/s/Hz. The SI-CAP maintains its performance gain at higher constellation and spectral efficiency as shown in Fig. 5 (b) using M = 16 to achieve $\mathcal{T}$ = 4 bpcu. From the Fig. 5 (b), the γ_b required by SI-CAP to achieve η = 15 bits/s/Hz is 1.6 dB less than that of m-CAP. This

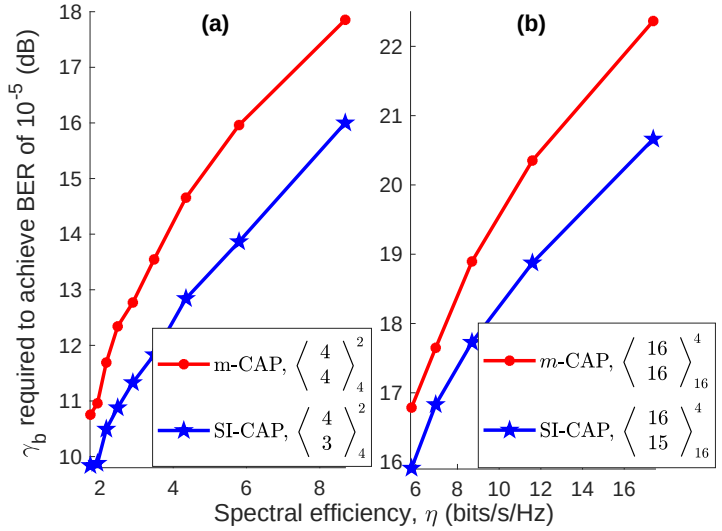

Fig. 5. Comparison of the γ_b required by SI-CAP and m-CAP to achieve BER of 10^{-5} in a bandwidth-limited VLC system modelled using a first-order low pass filter with $\mathcal{T}$ = 2 and 4 bpcu.

illustration shows the power/spectral efficiency gain of SI-CAP over the conventional m-CAP. The performance gain shown by the simulations is further validated through experimental demonstrations in Section V.

The complimentary cumulative distribution function (CCDF) of the electrical peak-to-average power (PAPR) of SI-CAP and m-CAP is investigated and shown in Fig. 6. The CCDF is defined as the probability that the PAPR exceeds a certain reference value PAPR_0 [21]. In order to investigate the PAPR of both schemes, we define the electrical PAPR per each transmitted symbol as:

$$PAPR \triangleq \frac{\max\limits_{0\le l\le L-1} |p(l)|^2}{E[|p(l)|^2]} \tag{23}$$

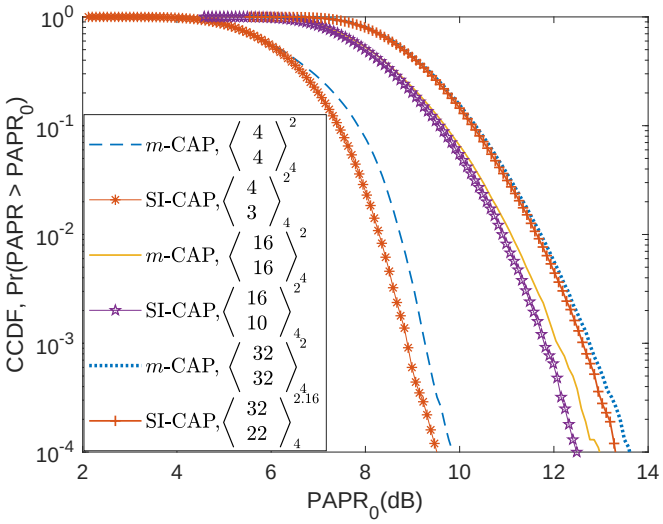

Fig. 6. The CCDF of the PAPR of SI-CAP and m-CAP for different number of subbands and transmission efficiencies.

where $p(l)$ is the lth sample of a symbol, L is the number of samples per symbol while $E[\cdot]$ denotes the statistical expectation. Though Fig. 6 shows that both SI-CAP and m-CAP exhibit comparable PAPR, a closer observation reveals that the PAPR of SI-CAP is marginally better especially in the region of interest for m-CAP. For example, the probability that the PAPR will exceed 9 dB is 6×10^{-4} and 3.5×10^{-3} respectively for SI-CAP and m-CAP using 4-QAM with $N = 4$ and $\mathcal{T} = 2$ bpcu. This means that out of every $10,000$ symbols, only 6 are likely to have their PAPR exceed 9 dB for SI-CAP as opposed to 35 for m-CAP. The PAPR of the two schemes becomes similar as N increases. However, it has been experimentally demonstrated that performance gain obtained when number of subbands is increased for m-CAP is marginal while the complexity becomes significant [22], [23]. This makes the lower PAPR exhibited by SI-CAP at lower value of N desirable.

V. Experimental Validation of SI-CAP Performance

The performance of the proposed SI-CAP is validated through experimental demonstrations using both VLC and SI-POF links. The illustration of the experiment set-up is shown in Fig. 7. For the VLC link, a high brightness blue LED (OSRAM LDCN5M) is used with a -3 dB cut-off frequency of 10.8 MHz as shown in Fig. 8 [24]. This VLC link introduces ISI in the the transmitted symbols at high spectral efficiency due to its limited modulation bandwidth. Similarly, the SI-POF link uses a 10 m SI-POF which introduces non-linearity effect as well as ISI. A resonant-cavity LED (RCLED, HAMAMATSU L10762) whose frequency response is shown in Fig. 8 is employed for the SI-POF demonstration [25].

Both the SI-CAP and m-CAP signals are generated offline on a computer and loaded onto an arbitrary waveform generator (AWG, Agilent 33600 series) that has a sample

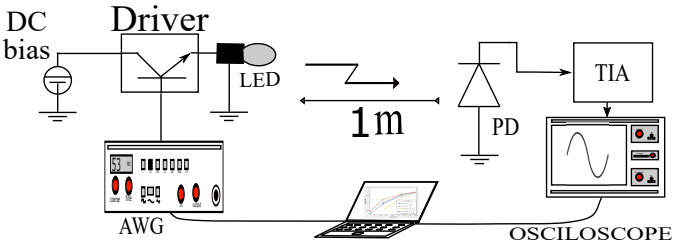

Fig. 7. Illustration of the set-up for the experimental demonstration.

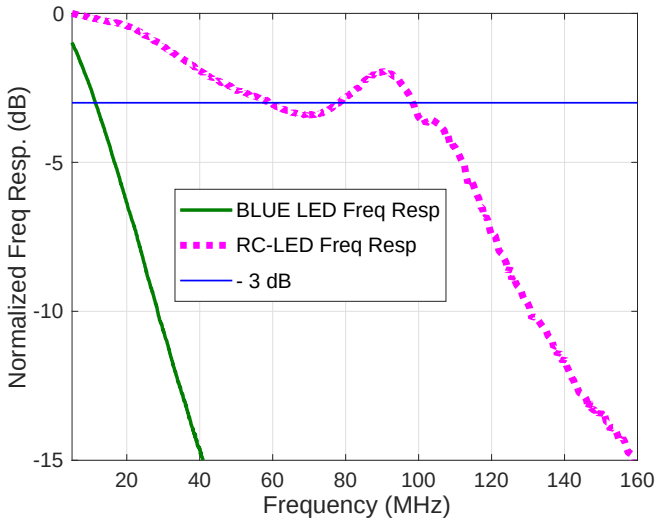

Fig. 8. The measured normalized frequency responses of the Blue and RC-LED employed for VLC and SI-POF experimental demonstration.

rate of 1 GSa/s and bandwidth of 120 MHz. The continuous waveform generated by the AWG is forwarded to a Bias-T where it is diplexed with a bias from a DC power supply to drive the optical source. Focussing lens are deployed at both the transmiting and receiving end of the VLC link to focus the data-bearing optical intensity on the receiving photodiode (PD). The PD, which is employed for both the VLC and SI-POF link, is a silicon PIN detector (THORLABS PDA10A(-EC)) with an active area of 0.8 mm^2, bandwidth of 150 MHz and a root mean square (RMS) noise of 1.5 mV [26]. It has responsivity, $\Re$, of 0.19 A/W and 0.41 A/W at the 460 nm and 660 nm of the blue LED and RCLED, respectively.

The received signal from the PD is captured in real time by an oscilloscope (Agilent 7000B Series) with a maximum sample rate of 4 GSa/s and 1 GHz bandwidth. The signal is then processed offline using the SI-CAP and m-CAP receivers previously described. In addition, an adaptive, symbol-spaced recursive least square (RLS) equalizer with 12 taps is implemented for the two schemes to further improve the achievable spectral efficiency.

The performance of the two schemes in VLC system is presented in Fig. 9 along with the equalization results. The modulation index, β, of the transmitted signal is set at 0.39. The proposed SI-CAP has a better performance over the range of spectral efficiencies investigated. At the FEC BER limit of 3×10^{-3}, the SI-CAP achieves $\eta = 8.6$ bits/s/Hz

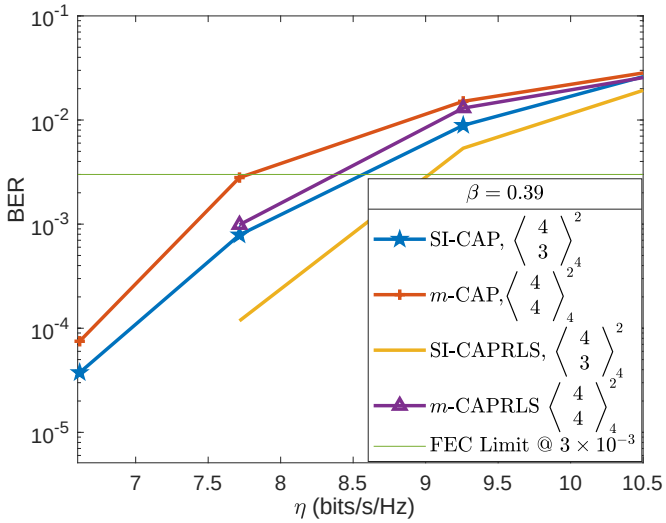

Fig. 9. Experimental demonstration of the performance of SI-CAP and m-CAP over a VLC link, $\beta = 0.39$.

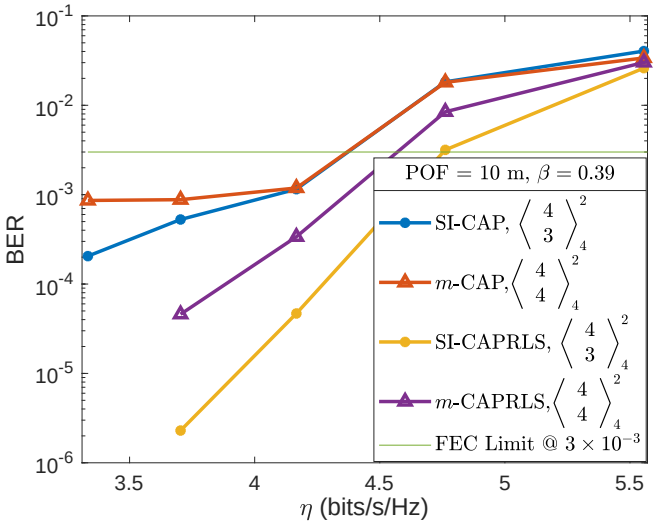

Fig. 11. Experimental demonstration of SI-CAP and m-CAP over a 10 m SI-POF link employing RCLED, $\beta = 0.39$.

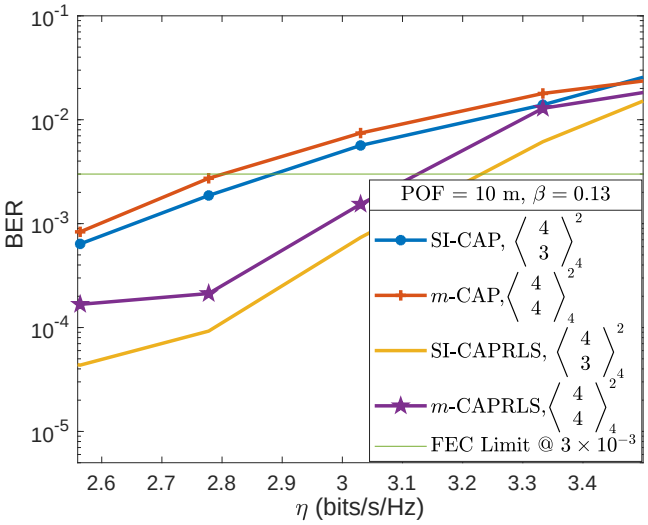

Fig. 10. Experimental demonstration of SI-CAP and m-CAP over a 10 m SI-POF link employing RCLED, $\beta = 0.13$.

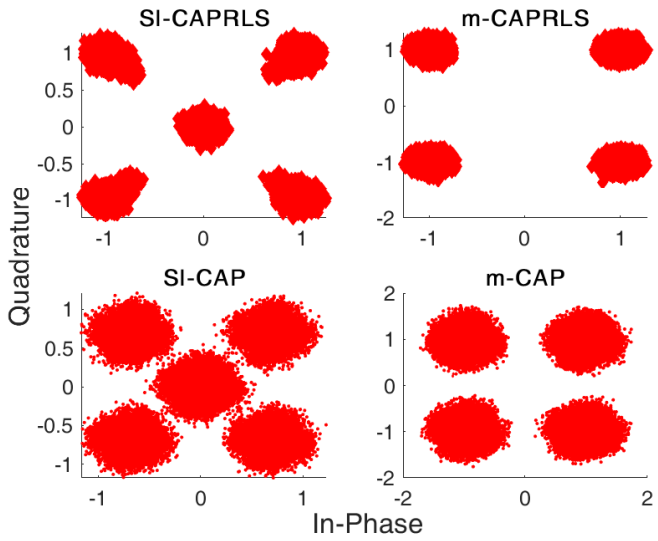

Fig. 12. Constellation plots of the proposed SI-CAP and the conventional $m-$CAP before and after equalization in SI-POF link, $\mathcal{T} = 2$ bpcu, $\eta = 4.2$ bits/s/Hz and $\beta = 0.39$.

in comparison to 7.8 bits/s/Hz achieved by m-CAP. This translates to spectral efficiency gain of 0.8 bits/s/Hz. At the same FEC limit, the RLS equalizer improves the η gain of both schemes by approximately 0.6 bits/s/Hz with SI-CAP maintaining its performance advantage.

To further show the versatility of SI-CAP, its performance is investigated in SI-POF link. The results are shown in Figs. 10 and 11 corresponding to $\beta = 0.13$ and 0.39, respectively. At $\beta = 0.13$ and the FEC BER limit, SI-CAP achieves η of 2.88 bits/s/Hz in comparison to 2.8 bits/s/Hz by m-CAP. On implementation of RLS equalizer, the η of SI-CAP increases by 0.5 bits/s/Hz while m-CAP increases by 0.3 bits/s/Hz. The performance of the two schemes are identical when the β increases to 0.39 with both achieving η of 4.37 bits/s/Hz at the FEC BER limit. However, SI-CAP has a higher gain when RLS equalizer is applied as it achieves η gain of 0.4 bits/s/Hz in comparison to 0.2 bits/s/Hz achieved by m-CAP.

Constellation plots of the two schemes in SI-POF link are shown in Fig. 12 for the equalised and unequalised case with $\mathcal{T} = 2$ bpcu and $\eta = 4.2$ bits/s/Hz. The feedforward symbol-spaced RLS equalizer considered shows that the achievable gain of SI-CAP can be enhanced with equalization schemes. To further enhance the gain, decision feedback equalizers can also be implemented. However, these constellation plots highlight the distinct difference between SI-CAP and m-CAP signals. The plots show an extra level in the constellation of SI-CAP which corresponds to the zeros transmitted on the inactive subbands. This additional constellation point at the origin means the SI-CAP will require extra consideration when designing equalization schemes such

as those with decision feedback configuration. This is because decisions on zeros, in addition to the QAM levels, will need to be fed back to the equalizer. Alternatively, different signal constellation pattern might be transmitted on the inactive subbands instead of zeros which will further enhance the transmission efficiency of the SI-CAP system by trading off the energy efficiency. These considerations and others are currently being investigated to improve on the SI-CAP proposed in this work.

VI. Conclusion

A subband index carrierless amplitude and phase modulation scheme (SI-CAP) has been developed and investigated for optical communication systems in this work. The proposed SI-CAP not only modulate data symbols on the subbands of a multi-band CAP scheme, but also conveys additional information bits on the index of those subbands. A theoretical BER expression is derived for the proposed SI-CAP and validated through simulation. In addition, a new detection scheme that achieves ML solution at lower complexity is developed for the proposed SI-CAP. The SI-CAP performance is investigated for optical systems including VLC and SI-POF links through simulations and experimental demonstrations. It is shown that for the same spectral efficiency, SI-CAP requires lower SNR per bit to achieve the same BER performance as m-CAP. Alternatively, if the SNR per bit is fixed for both schemes, SI-CAP achieves a higher spectral efficiency. Furthermore, a feedforward adaptive RLS equalization scheme is implemented to further enhance the achievable gain of SI-CAP. Therefore, the superior performance of SI-CAP over the conventional m-CAP and its design flexibility make it a suitable candidate for optical communication systems.

References

[1] Z. Ghassemlooy, W. Popoola, and S. Rajbhandari, *Optical Wireless Communications: System and Channel Modelling with MATLAB*, 1st ed. Boca Raton, FL, USA: CRC Press, Inc., 2012.

[2] I. N. Osahon, S. Rajbhandari, and W. O. Popoola, "Performance comparison of equalization techniques for SI-POF multi-gigabit communication with PAM- M and device non-linearities," *Journal of Lightwave Technology*, vol. 36, no. 11, pp. 2301–2308, June 2018.

[3] D. Karunatilaka, F. Zafar, V. Kalavally, and R. Parthiban, "LED based indoor visible light communications: State of the art," *IEEE Communications Surveys Tutorials*, vol. 17, no. 3, pp. 1649–1678, thirdquarter 2015.

[4] W. O. Popoola, "Impact of VLC on light emission quality of white LEDs," *Journal of Lightwave Technology*, vol. 34, pp. 2526–2532, 2016.

[5] I. N. Osahon, E. Pikasis, S. Rajbhandari, and W. O. Popoola, "Hybrid POF/VLC link with M-PAM and MLP equaliser," in *2017 IEEE International Conference on Communications (ICC)*, May 2017, pp. 1–6.

[6] J. Zubia and J. Arrue, "Plastic optical fibers: An introduction to their technological processes and applications," *Optical Fiber Technology*, vol. 7, no. 2, pp. 101 – 140, 2001.

[7] S. Liang, Z. Jiang, L. Qiao, X. Lu, and N. Chi, "Faster-than-nyquist precoded CAP modulation visible light communication system based on nonlinear weighted look-up table predistortion," *IEEE Photonics Journal*, vol. 10, no. 1, pp. 1–9, Feb 2018.

[8] Y. Wang, L. Tao, X. Huang, J. Shi, and N. Chi, "8-Gb/s RGBY LED-based WDM VLC system employing high-order CAP modulation and hybrid post equalizer," *IEEE Photonics Journal*, vol. 7, no. 6, pp. 1–7, Dec 2015.

[9] C. C. Wei, K. Z. Chen, L. W. Chen, C. Y. Lin, W. J. Huang, and J. Chen, "High-capacity carrierless amplitude and phase modulation for WDM long-reach PON featuring high loss budget," *Journal of Lightwave Technology*, vol. 35, no. 4, pp. 1075–1082, Feb 2017.

[10] K. O. Akande and W. O. Popoola, "MIMO techniques for carrierless amplitude and phase modulation in visible light communication," *IEEE Communications Letters*, vol. PP, no. 99, pp. 1–1, 2018.

[11] K. Werfli, P. Chvojka, Z. Ghassemlooy, N. B. Hassan, S. Zvanovec, A. Burton, P. A. Haigh, and M. R. Bhatnagar, "Experimental demonstration of high-speed 4×4 imaging multi-CAP MIMO visible light communications," *Journal of Lightwave Technology*, vol. 36, no. 10, pp. 1944–1951, May 2018.

[12] W. O. Popoola, "Merits and limitations of spatial modulation for optical wireless communications," in *2013 2nd International Workshop on Optical Wireless Communications (IWOW)*, Oct 2013, pp. 152–156.

[13] P. A. Haigh *et al.*, "A multi-CAP visible-light communications system with 4.85-b/s/Hz spectral efficiency," *IEEE Journal on Selected Areas in Communications*, vol. 33, no. 9, pp. 1771–1779, Sept 2015.

[14] M. I. Olmedo, T. Zuo, J. B. Jensen, Q. Zhong, X. Xu, S. Popov, and I. T. Monroy, "Multiband carrierless amplitude and phase modulation for high capacity optical data links," *Journal of Lightwave Technology*, vol. 32, no. 4, pp. 798–804, Feb 2014.

[15] P. A. Haigh *et al.*, "Multi-band carrier-less amplitude and phase modulation for bandlimited visible light communications systems," *IEEE Wireless Communications*, vol. 22, no. 2, pp. 46–53, April 2015.

[16] E. Baar, . Aygl, E. Panayrc, and H. V. Poor, "Orthogonal frequency division multiplexing with index modulation," in *2012 IEEE Global Communications Conference (GLOBECOM)*, Dec 2012, pp. 4741–4746.

[17] J. G. Proakis, *Digital Communications, (4th Ed)*. New York: McGraw-Hill, 2001.

[18] E. Basar, "Orbital angular momentum with index modulation," *IEEE Transactions on Wireless Communications*, vol. 17, no. 3, pp. 2029–2037, March 2018.

[19] T. Mao, Z. Wang, Q. Wang, S. Chen, and L. Hanzo, "Dual-mode index modulation aided OFDM," *IEEE Access*, vol. 5, pp. 50–60, 2017.

[20] W. O. Popoola, E. Poves, and H. Haas, "Error performance of generalised space shift keying for indoor visible light communications," *IEEE Transactions on Communications*, vol. 61, no. 5, pp. 1968–1976, May 2013.

[21] W. O. Popoola, Z. Ghassemlooy, and B. G. Stewart, "Pilot-assisted PAPR reduction technique for optical OFDM communication systems," *Journal of Lightwave Technology*, vol. 32, no. 7, pp. 1374–1382, 2014.

[22] P. A. Haigh, E. Hugues-Salas, and J. Wei, "On the performance of increasing subcarrier order in multi-band carrier-less amplitude and phase modulation for short haul optical links," in *Asia Communications and Photonics Conference*. Optical Society of America, 2017, p. S4B.6.

[23] J. L. Wei, C. Sanchez, and E. Giacoumidis, "Fair comparison of complexity between a multi-band CAP and DMT for data center interconnects," *Opt. Lett.*, vol. 42, no. 19, pp. 3860–3863, Oct 2017.

[24] O. O. Semiconductors, *OSLON SX Datasheet*, Nov. 2012, ver 1.1.

[25] HAMAMATSU, *Resonant cavity LED for POF data communication*, Feb. 2016.

[26] THORLABS, *Si Amplified Fixed Gain Detector*, Sept. 2017, rev. J.